

## Chapter 4

### Imaging

#### 4.1 Near resonance - absorption imaging

For a majority of the experiments described in this thesis, absorption imaging has been employed. This has been covered in detail in Ensher's thesis [61], but a few additional aspects are addressed here. Essentially, absorption imaging relies on the resonant scattering of light out of a probe beam, and the decrease in probe beam intensity is measured. Intensity decays exponentially through the condensate;  $I_m = I_0 e^{-OD}$ . The optical depth represents the column density of atoms along the probe direction;  $OD(\vec{r}) = \int n(\vec{r}, \vec{z}) \sigma_0 d\vec{z}$  for the scattering cross-section  $\sigma_0$ . It is extracted by imaging the spatially dependent probe intensity onto a CCD through the following three pictures;  $I_{\text{shadow}}$  – the intensity profile with the condensate present,  $I_{\text{light}}$  – the intensity profile of the probe beam only, and  $I_{\text{dark}}$  – an image with the probe beam off, so that only external sources of offsets are measured (for example, dark current on the CCD, or room lights). The measured optical depth is then calculated through

$$OD_{\text{meas}}(\vec{r}) = \ln \left( \frac{I_{\text{light}}(\vec{r}) - I_{\text{dark}}(\vec{r})}{I_{\text{shadow}}(\vec{r}) - I_{\text{dark}}(\vec{r})} \right). \quad (4.1)$$

This equation is applied for each pixel on the CCD array. For probe intensities comparable to the saturation intensity (1.6 mW/cm<sup>2</sup>), the absorption no longer follows this equation, and Ensher [61] has derived a correction to obtain the real

optical depth from the measured  $OD_{\text{meas}}(\vec{r})$  and the probe intensity.

There are two more effects worth mentioning. The first has to do with a general correction which can be applied to account for many effects. Since the previous formulae rely on the assumption that all of the probe light interacts with the atoms the same way, the presence of off-resonant or incorrectly polarized light will lead to systematic effects. Since the probe laser linewidth is much less than the atomic linewidth, the light can be broken up into two pieces; on-resonant and correctly polarized light, off-resonant, incorrectly polarized, or scattered light. The first piece is the probe light which provides a signal proportional to the column density through the condensate. The remaining pieces are part of the probe beam but cannot be absorbed by the atoms. These can be lumped together into  $\alpha$ , the fraction of the intensity which is not absorbed, and treated the same way as the other offsets  $I_{\text{dark}}$ . The measured optical depth using Eq. 4.1 becomes

$$OD_{\text{meas}}(\vec{r}) = \ln \left( \frac{I_{\text{light}}(\vec{r}) - I_{\text{dark}}(\vec{r})}{I_{\text{shadow}}(\vec{r}) + \alpha I_{\text{light}}(\vec{r}) - I_{\text{dark}}(\vec{r})} \right). \quad (4.2)$$

It is not practical to directly measure  $\alpha I_{\text{light}}(\vec{r})$  simply through another image on the CCD, so its value must be found through other means. Once it is measured, the following rearrangement of Eq. 4.2 may be applied on a pixel by pixel basis to get the actual optical depth:

$$OD_{\text{real}}(\vec{r}) = OD_{\text{meas}}(\vec{r}) - \ln \left( 1 - \alpha(\vec{r}) e^{OD_{\text{meas}}(\vec{r})} \right) + \ln(1 - \alpha(\vec{r})). \quad (4.3)$$

This is plotted in Fig. 4.1 for three values of  $\alpha$ .

An example of the above correction is the “polarization correction”, which accounts for the variation in the direction of the atoms’ quantization axis as the TOP field rotates during the probing. Ideally, the probing would only occur while the TOP field points along (or toward) the circularly polarized probe beam so that the cycling transition  $F = 2, m_F = 2 \rightarrow F' = 3, m_F = 3$  is driven. Since the

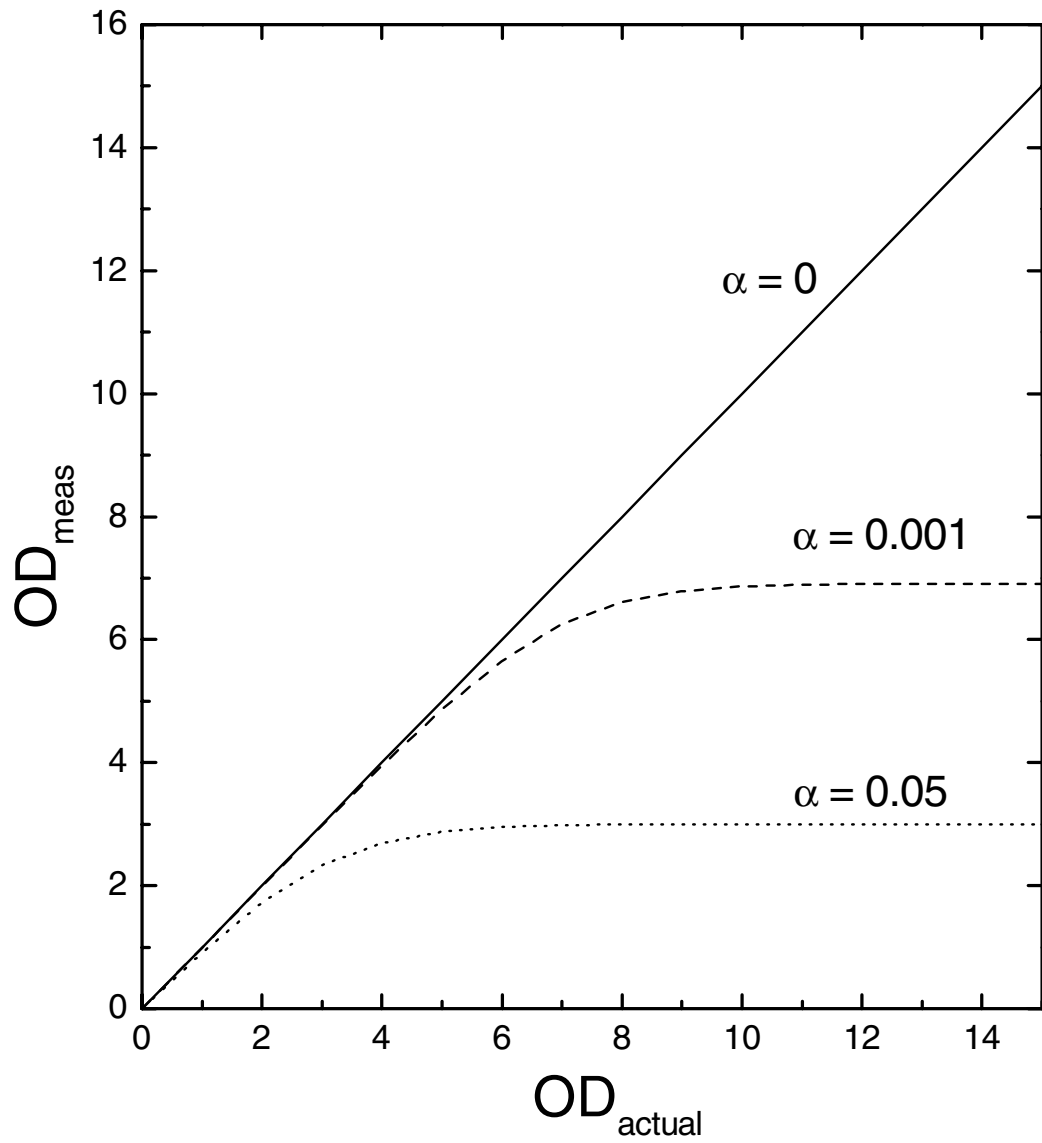


Figure 4.1: For a real optical depth of  $OD_{\text{actual}}$  the observed value ( $OD_{\text{meas}}$ ) is plotted for different values of the fraction of light which cannot be absorbed by the atoms  $\alpha$ .

probe has finite duration  $t_p$ , the field rotating at angular frequency  $\omega_t$  sweeps out an angle  $\theta = t_p\omega_t$ . This can either be thought of as a time-varying polarization applied to the  $m_F = 2$  state, or as a constant circular polarization applied to a time-varying state superposition. In the second picture the population in the  $m_F = 2$  state varies as  $\cos^4(\theta/2)$ . Integrating this from  $-\theta/2 \rightarrow \theta/2$  (assumes that the TOP field points along the probe beam half-way through the probe pulse) gives the fraction of correctly polarized light (*i.e.*  $= 1 - \alpha$ ) :

$$\begin{aligned} f &= \frac{3}{8} + \frac{1}{\theta} \cos^3\left(\frac{\theta}{4}\right) \sin\left(\frac{\theta}{4}\right) + \frac{3}{2\theta} \cos\left(\frac{\theta}{4}\right) \\ &\simeq 1 - \frac{1}{24}\theta^2 + \frac{1}{768}\theta^4 \end{aligned} \quad (4.4)$$

for small  $\theta$ . The resulting incorrectly polarized fraction can be substituted into Eq. 4.3 for alpha. In early experiments where  $\omega_t = 2\pi \times 7200$  Hz and  $t_p = 25.7\mu\text{s}$ , this accounted for a 10% decrease in observed optical depth for a condensate with real optical depth of 1. This does not take into account other possible transitions.

#### 4.1.1 Lensing

Part of the simple model of absorption imaging is that the light traveling through the condensate is only attenuated by resonant scattering. For sufficiently dense atom clouds, there can also be a large spatial change in the index of refraction. The rays traveling through the cloud will suffer some refraction due to the curvature of the condensate, as well as its density profile. In this way it behaves as both a geometric lens and a gradient-index (GRIN) lens. The type of lens (converging or diverging) depends on the detuning of the probe from resonance as the index is greater or less than one respectively. This behavior can lead to systematics in measurements of the temperature and density. The focal length of

a ball of radius  $R$  with uniform density is given by

$$f = \frac{R}{2(n-1)} \quad (4.5)$$

where  $n$  is the index of refraction (see Eq. 4.10). Lensing is a problem when the focal length is shorter than the focal depth of the imaging system, or when the imaging system is improperly focused. For our imaging setup with an f-number of  $\sim 5$ , the focal depth is  $200 \mu\text{m}$ . A condensate of  $20 \mu\text{m}$  radius implies that  $(n-1) \ll .05$  for minimal lensing, which occurs for a probe detuning  $\Delta > 600$  MHz. At this detuning the observed optical depth is down to 0.05, which is visible but with signal to noise near unity.

A schematic of lensing is shown in Fig. 4.2. The condensate is represented by the dark grey ball and the probe beam is incident from the left. For the blue detuned case, the index is less than 1 so the condensate is a diverging lens. The solid lines represent the path of the probe light and the dashed lines show the boundary outside which the light does not travel through the condensate. At position B, light from the inside of the condensate is refracted outside the cylinder defined by the dashed boundary. Where this occurs (represented by the light grey areas) there is more light than the non-refracting model would suggest. If the focal plane of the imaging system were at B, the resulting optical depth would look basically normal near the center of the condensate (except for an enhanced OD), but would actually go negative at the edges due to the increase in light in the presence of a condensate. If the focal plane were at position A, then the virtual image must be taken into account, represented by the dotted lines. Here there is a cone of excess light, and the resulting optical depth has a corresponding negative dip in the center. Similar but reversed pictures occur in the case of red detuning.

Lensing is a serious complication when probing a condensate in the magnetic

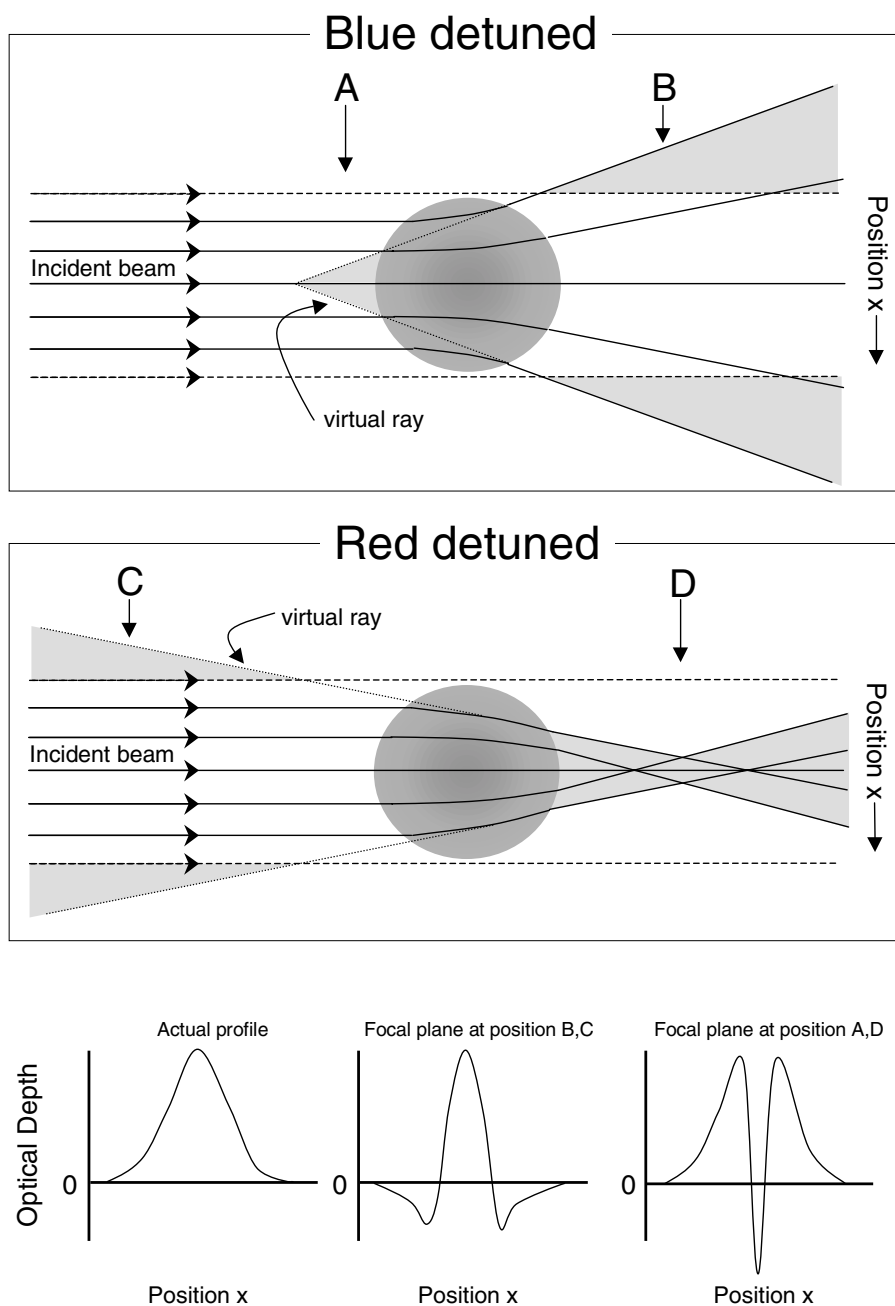


Figure 4.2: Schematic of a uniform ball with index  $\neq 1$  in the path of a probe beam incident from the left. Grey regions enclosed by beam paths indicate an increase in the light level over the non-refracting model. Regions outside the dashed lines (a cylinder around the condensate) are where the probe light does not intercept the condensate. Dotted lines represent virtual rays. At the bottom are the actual image in the absence of lensing, and the observed optical depth is shown for various focal plane locations.

trap. On resonance, the index is 1 so lensing is not a problem. However the optical depth is much too large ( $> 100$ ), so that small contributions to  $\alpha$  in Eq. 4.3 can severely effect the optical depth, leading to a saturation. In fact, from Eq. 4.3 the maximum observable optical depth is

$$OD_{\max} = \ln\left(\frac{1}{\alpha}\right) \quad (4.6)$$

which turns out to be  $\sim 3$  for our experiment, implying  $\alpha = .05$ . Detuning further from resonance does make lensing better, but the index of refraction only drops off as  $1/\Delta$  and the signal drops as  $1/\Delta^2$  so the “signal-to-lensing” ratio gets worse. For this reason destructive imaging is most useful when looking at dropped, expanded condensates when the density is low and the radius of curvature big.

#### 4.1.2 Signal-to-noise

The signal-to-noise is given in terms of the real optical depth by;

$$S/N = \frac{OD_{\Delta}(1 - \alpha) \exp^{-OD_{\Delta}}}{\sqrt{\sigma_S^2 + \sigma_L^2} ((1 - \alpha) \exp(-OD_{\Delta}) + \alpha)} \quad (4.7)$$

where  $OD_{\Delta} = OD_{\text{res}}/(1 + 4(\Delta/\gamma)^2)$  for the on-resonance, real optical depth  $OD_{\text{res}}$ ,  $\Delta$  is the detuning from resonance,  $\gamma$  is the natural linewidth of  $^{87}\text{Rb}$  (5.9 MHz), and  $\sigma_L$  and  $\sigma_S$  is the fractional intensity noise in the light and shadow frames respectively. Noise on the dark frame is ignored in this analysis. This is justified since dark noise is about 1 count versus 7 counts of noise from the other sources listed here (dark noise can vary from chip to chip even for the same type, depending on CCD quality, the quality of the vacuum, and the temperature of the CCD). In the case of shot noise,  $\sigma_S = 1/\sqrt{(1 - \alpha)I_0 \exp(-OD_{\Delta}) + \alpha I_0}$  and  $\sigma_L = 1/\sqrt{I_0}$  and the signal-to-noise becomes

$$S/N_{\text{shot}} = \frac{\sqrt{I_0} OD_{\Delta}(1 - \alpha) \exp^{-OD_{\Delta}}}{\sqrt{(1 - \alpha) \exp(-OD_{\Delta}) + \alpha + 1} \sqrt{(1 - \alpha) \exp(-OD_{\Delta}) + \alpha}} \quad (4.8)$$

where  $I_0$  represents the number of photons in the probe (actually, it must also include the quantum efficiency of the detector). Since the signal for near-resonance imaging is a reduction in light level, the  $S/N_{\text{shot}}$  actually gets worse for large signals. The optical depth with maximum  $S/N_{\text{shot}}$  is 2.2 when  $\alpha = 0$ , implying that the detuning  $\Delta$  should be set to achieve that measured  $OD$ . Figure 4.3 shows the optimal optical depth for different values of  $\alpha$ .

A major source of noise above shot noise for usual intensities is spatial fluctuations of the probe intensity between the shadow and light frames. This is due to small scale fringes on the probe beam that change position between the  $I_{\text{shadow}}$  and  $I_{\text{light}}$ . In this case the noise is linear in the light intensity, and  $\sigma$  is the standard deviation for a sinusoidal function with fractional amplitude  $A$ . The signal-to-noise is

$$S/N_{\text{fringe}} = \frac{\sqrt{2}}{A} \frac{OD_{\Delta}(1 - \alpha) \exp^{-OD_{\Delta}}}{((1 - \alpha) \exp(-OD_{\Delta}) + \alpha)} \quad (4.9)$$

assuming maximum variation in the fringe spacing. The optimal optical depth in this case is also plotted in Fig. 4.3. These are compared to other imaging techniques at the end of this chapter.

### 4.1.3 Magnification measurement

For many quantitative measurements knowing the imaging magnification is extremely important. If an atom cloud is to be used for measuring the magnification, then the camera must be set at the focal point of the imaging system. Ensher [61] described a method for doing this by destructively imaging small atom clouds in the magnetic trap. This technique was plagued by lensing effects and gave only modest results. Non-destructive imaging brought the ability to tolerate large optical depths so that very small clouds could be imaged in the trap. The position of the camera was then adjusted to give the smallest observed cloud

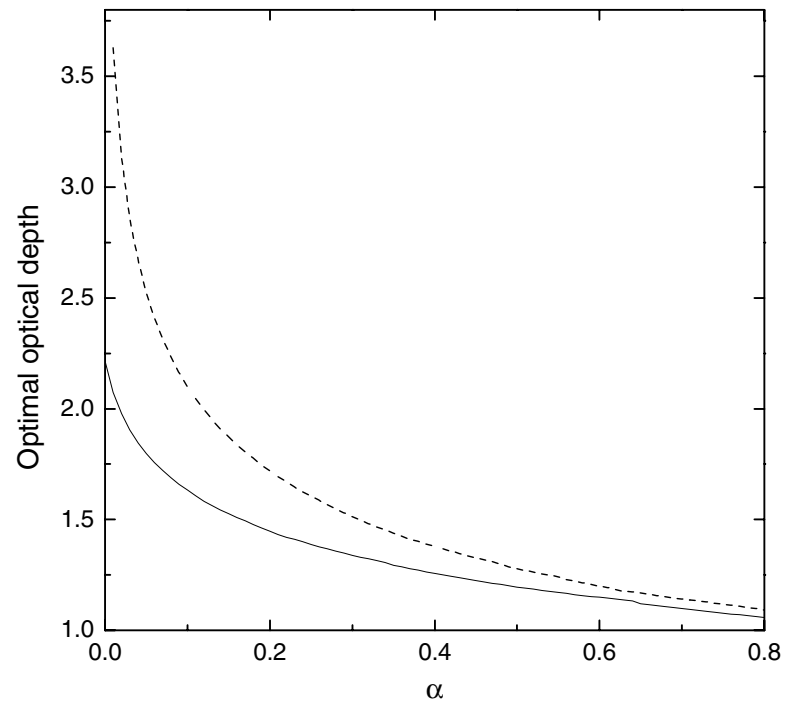


Figure 4.3:  $\alpha$  is the fraction of the probe intensity which cannot be absorbed by the atoms. This plot shows the optical depth required for the best signal to noise for a given value of  $\alpha$  in the shot noise limit (solid line) and for the intensity noise limit (dashed line).

diameter.

The first method used for a magnification measurement was to obtain a value for  $g$  by turning off the trap and watching the atom cloud fall. A new picture was taken for each different time after the trap was turned off. The resulting vertical position was fit to a gravitational acceleration with a size scaling, and an initial velocity. The size scaling directly gives the magnification.

A separate method for measuring the magnification was to use the interference of two beams which cross at the same location of the atom cloud, as illustrated in Fig. 4.4. Essentially, the input angle  $\alpha$  was measured, and the fringe spacing from the interference on the CCD was measured to yield the angle  $\beta$ . The magnification is then the ratio  $\alpha/\beta$ . It is crucial that the two beams cross at the location of the atom cloud. This was done by first centering the probe beam on the atoms. While looking at the CCD image, the split-off beam (dotted line) was overlapped with the probe beam on the CCD, guaranteeing that they crossed at the atom cloud since the imaging system was previously set at the focal point for the cloud. The current magnification from this method is 9.4, or 1 camera pixel =  $2.5\mu\text{m}$  in the trap. This method and the dropping method yield very similar results, so one is not clearly better than the other. They are complimentary though since they rely on very different measurements. A possible systematic affecting the optical measurement is curvature in the glass windows that changes the angle between the two beams before the lens L1. This effect could be manifested in different ways between the optical method and dropping method, since they use different axes and regions of the window(s).

#### 4.1.4 Double condensate imaging

Early double condensate experiments used destructive imaging of ballistically expanded condensates. Ensher [61] provides an explanation of the sequence

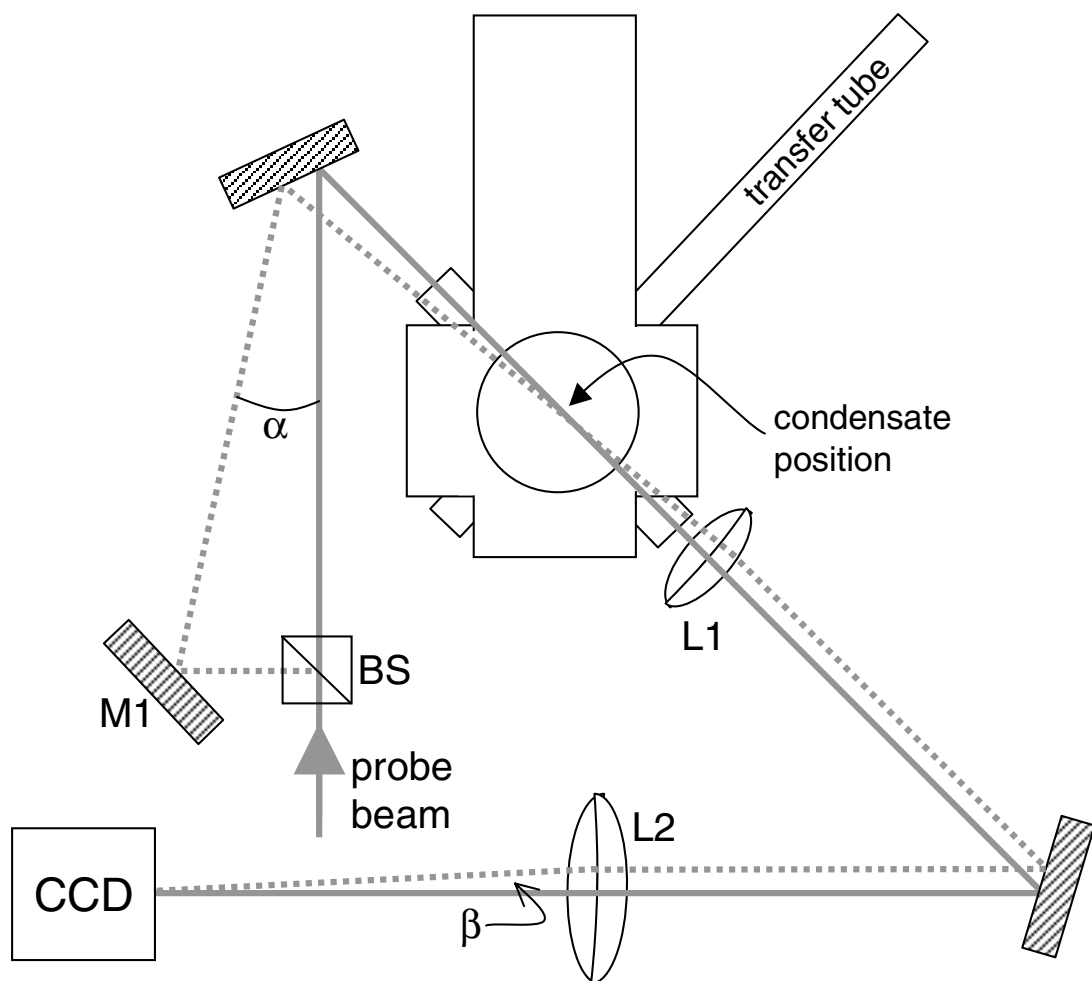


Figure 4.4: A schematic for measurement of the imaging system magnification using interference. The probe beam is split into two pieces which cross with angle  $\alpha$  where the condensate would be. They overlap again on the CCD array, but at a different angle  $\beta$ , measured by observing the fringe spacing of the interference pattern on the CCD. The ratio of  $\alpha/\beta$  determines the magnification.

of laser pulses necessary to see either of the  $|1, -1\rangle$  or  $|2, 1\rangle$  states. However, to image  $|1, -1\rangle$  in the presence of  $|2, 1\rangle$  it was necessary to “blow away” the  $|2, 1\rangle$  atoms with a  $\sim 2$  ms pulse of MOT light about 10 ms before the  $|1, -1\rangle$  atoms were imaged (the expansion time was typically 22 ms, so the MOT pulse occurred after  $\sim 12$  ms of expansion). For significant attenuation ( $8 \times 10^{-3}$ ) of the MOT beams this was sufficient to not disturb the  $|1, -1\rangle$  atoms.

In order to image both states in a single shot a similar technique was used. The  $|2, 1\rangle$  atoms were first imaged using a  $F = 2 \rightarrow F' = 3$  probe pulse. About 1 ms later the attenuated MOT light was flashed on for 2.8 ms to discard the  $|2, 1\rangle$  atoms as described above. One millisecond after that, the  $|1, -1\rangle$  atoms were imaged by applying a short repump pulse and then the probe pulse [61]. Since there is significant time between the imaging of the states, the  $|1, -1\rangle$  condensate expands and drops further as seen in Fig. 4.5.

## 4.2 Polarization Imaging

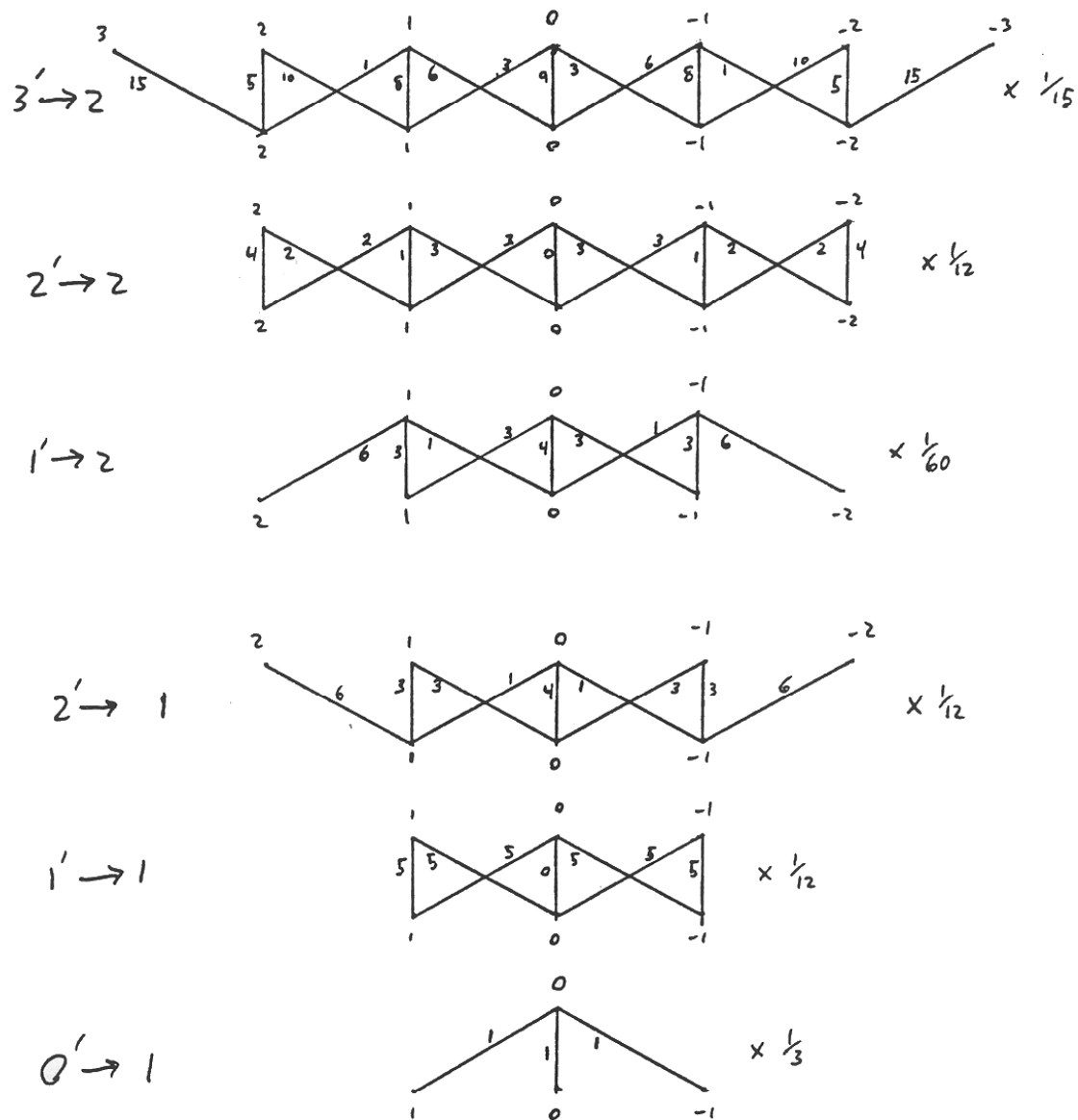
Polarization imaging was used as a first attempt at non-destructive imaging of a condensate. When a condensate is in a single state, the Clebsh-Gordon coefficients  $K$  (Fig. 4.6 and Tab. 4.1) are in general different for left ( $\sigma_-$ ) and right ( $\sigma_+$ ) circularly polarized light. If the input probe beam is linearly polarized, then the output beam will have its polarization axis rotated slightly, since the  $\sigma^+$  and  $\sigma^-$  components experience different phase shifts through the condensate. This is the same birefringent process exploited in polarization spectroscopy [55].

For light with frequency  $\omega$  and detuning  $\Delta$  from the atomic transition, the phase shift [10] through a media of length  $d$  is

$$\begin{aligned} \phi &= \frac{d\omega}{c} \text{Re}(n(\Delta)) \\ \text{Re}(n(\Delta)) &= 1 + \frac{Ne^2}{8\pi\epsilon_0 m\omega} \sum_i \frac{\Delta_i}{\Delta_i^2 + (\gamma/2)^2} K_i \end{aligned} \quad (4.10)$$



Figure 4.5: Image of both the  $|2, 1\rangle$  (top) and  $|1, -1\rangle$  (bottom) condensates after dropped from the magnetic trap. In the trap the  $|2, 1\rangle$  sits below the  $|1, -1\rangle$ .

Figure 4.6: Branching ratios for  $^{87}\text{Rb}$ .

state	$\sigma_+$	$\sigma_-$	$\pi$
$ 2, 2\rangle$	1/2	1/6	1/3
$ 2, 1\rangle$	5/12	1/4	1/3
$ 1, -1\rangle$	5/12	1/4	1/3

Table 4.1: The effective Clebsh-Gordon coefficients for light far detuned from the  $5P_{3/2}$  states.

where  $Nd$  is the integrated through density,  $e$  and  $m$  are the charge and mass of the electron and the sum is over all possible transitions. It must also be true that the Clebsh-Gordon coefficients are normalized  $\sum_i K_i = 1$ . Specializing to only two levels (for  $\sigma^+$  and  $\sigma^-$ ) which are assumed to be at nearly the same detuning from the initial state (as compared to  $\Delta$ ), the difference in phase shift is

$$\delta\phi = \sigma_0 \frac{Nd}{8\pi} \gamma \frac{\Delta}{\Delta^2 + (\gamma/2)^2} (K^+ - K^-) \quad (4.11)$$

in which  $\sigma_0$  is the on resonant cross-section for the atom to scatter a photon. Since the on-resonance optical depth is simply  $\sigma_0 Nd$ , this can be rewritten in order to compare with destructive imaging;

$$OD_{\text{res}} = \frac{8\pi}{(K^+ - K^-)} \frac{\Delta}{\gamma} \delta\phi \quad (4.12)$$

when  $\Delta \gg \gamma$ .

The setup to measure the rotation of polarization due to  $\delta\phi$  is shown in Fig. 4.7. A Glan-laser input polarizer (P1) defines the polarization of the incoming probe beam. The condensate is imaged when the rotating magnetic field has the correct phase to point along the probe beam so that the linear polarization is composed of equal parts  $\sigma^+$  and  $\sigma^-$ . A second Glan-laser polarizer (P2) at angle  $\theta$  to the first allows a measurement of the amount of rotation of the polarization. For an input intensity (after the first polarizer)  $I_0$  and a relative phase shift of  $\delta\phi$ , the polarization is rotated by  $\delta\phi/2$ . The intensity at the CCD is

$$I_m = I_0 \cos^2(\theta - \delta\phi/2). \quad (4.13)$$

As in the destructive measurements, three images are taken in order to measure the beam intensity distribution and any offsets. The optical depth can be written in terms of the measured quantities and applied on a pixel by pixel basis (similar to Eq. 4.1):

$$OD_{\text{res}} = \frac{16\pi}{(K^+ - K^-)} \frac{\Delta}{\gamma} \left( \cos^{-1} \sqrt{\frac{I_{\text{shadow}} - I_{\text{dark}}}{I_{\text{light}} - I_{\text{dark}}}} - \theta \right). \quad (4.14)$$

The quantity  $\delta\phi/(\sigma_0 N d)$  from Eq. 4.12 (using the full sum Eq. 4.10) is plotted in figure 4.8 for the three trapped states of  $^{87}\text{Rb}$ . In (c) data is shown for a non-condensed cloud of  $|2, 2\rangle$  atoms over regions of minimal scattering rate. For (c) the probe laser frequency was determined by measuring the beat frequency between it and the MOT laser with an avalanche photodiode.

This signal may be used for nondestructive measurements of double condensate systems. For large detunings ( $\Delta \gg \gamma$ ) from both the  $|2, 1\rangle$  and  $|1, -1\rangle$  states, the signal for atoms in either hyperfine state and the trappable  $m_F$  Zeeman state is

$$\delta\phi = \frac{OD_{\text{res}}}{8\pi} \frac{\gamma}{\Delta} \frac{|m_F|}{6} \quad (4.15)$$

where the presence of  $|m_F|$  is only a useful coincidence; it has no physical meaning. When the probe is tuned between the resonances for  $|1, -1\rangle$  and  $|2, 1\rangle$ , the signal is positive for  $|2, 1\rangle$  atoms and negative for  $|1, -1\rangle$  atoms since the detuning  $\Delta$  switches signs. This makes polarization imaging useful for double condensate measurements since the states are distinguishable. In this case the range of phase shift is the difference between all the atoms in  $|1, -1\rangle$  and all the atoms in  $|2, 1\rangle$ ;

$$\delta\phi = \frac{OD_{\text{res}}}{24\pi} \frac{\gamma}{\Delta}. \quad (4.16)$$

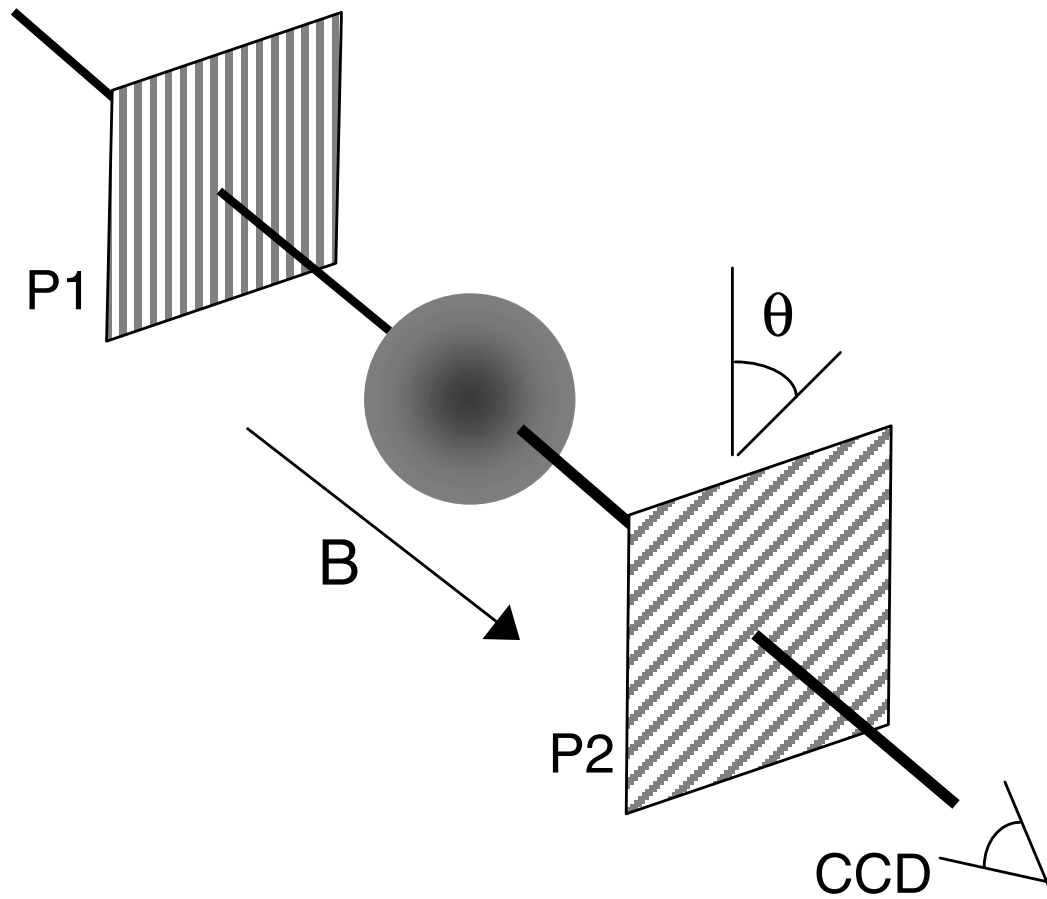


Figure 4.7: Schematic for polarization imaging. The probe beam incident from the upper-left travels through a polarizer (P1) to purify the polarization. It travels through the condensate whose birefringence rotates the polarization of the probe. The beam exits through the second polarizer (P2) which is at an angle  $\theta$  to the first. The transmission through P2 depends on the amount of polarization rotation caused by the condensate which is proportional to the column density.

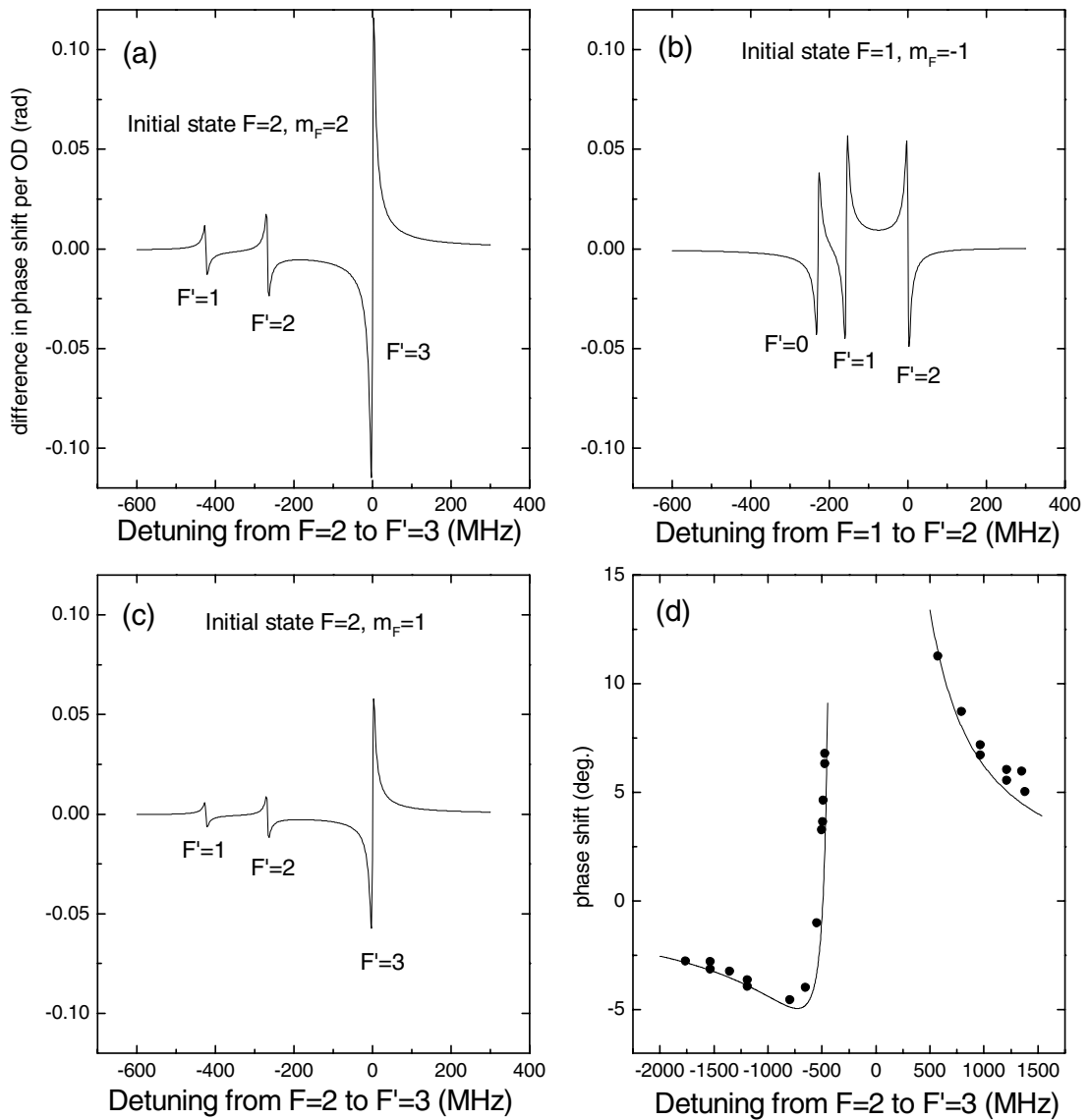


Figure 4.8: Plots of the signal from polarization imaging as a function of detuning. (a) For atoms in the  $F = 2, m_F = +2$  state. (b) For atoms in the  $F = 1, m_F = -1$  state. (c) For atoms in the  $F = 2, m_F = +1$  state. (d) Rotation of the probe's polarization as a function of detuning for atoms in the  $F = 2, m_F = +2$  state. The data points are for a cloud with optical depth  $\sim 70$ .

### 4.2.1 Signal-to-noise

The signal to noise for polarization imaging is

$$S/N = \delta\phi(\Delta, OD_{\text{res}}) \frac{\sin(\theta - \delta\phi(\Delta, OD_{\text{res}})/2)}{\cos(\theta - \delta\phi(\Delta, OD_{\text{res}})/2)} \frac{1}{\sqrt{\sigma_L^2 + \sigma_S^2}} \quad (4.17)$$

where  $\delta\phi(\Delta, OD_{\text{res}})$  is given in Eq. 4.11. For the shot noise limit on the probe intensity,  $\sigma_S^2 = 1/I_0 \cos^2(\theta - \delta\phi(\Delta, OD_{\text{res}}))$  and  $\sigma_L^2 = 1/I_0 \cos^2 \theta$  the signal to noise is

$$S/N_{\text{shot}} = \sqrt{I_0} \delta\phi(\Delta, OD_{\text{res}}) \frac{\sin(\theta - \delta\phi(\Delta, OD_{\text{res}})/2) \cos \theta}{\sqrt{\cos^2(\theta - \delta\phi(\Delta, OD_{\text{res}})) + \cos^2 \theta}} \quad (4.18)$$

When the noise is dominated by fringes with fractional amplitude  $A$  on the probe intensity, the signal to noise is simply

$$S/N_{\text{fringe}} = \delta\phi(\Delta, OD_{\text{res}}) \frac{\sin(\theta - \delta\phi(\Delta, OD_{\text{res}})/2)}{\cos(\theta - \delta\phi(\Delta, OD_{\text{res}})/2)} \frac{\sqrt{2}}{A} \quad (4.19)$$

Both of these have a maximum near  $\theta = \pi/2$  when the phase shift  $\delta\phi$  is small. Data was taken looking at a condensate expanded 10 ms from a 80 Hz axial frequency trap. Figure 4.9 shows this and a fit of the shot noise limiting form of Eq. 4.18.

Birefringence of the vacuum windows contributes an offset which can add to the noise. The birefringence was measured by rotating the input polarization with a waveplate, and correspondingly rotating the input polarizer. The output polarizer was then rotated to find the extinction ratio. It was found that the best extinction ratio was for vertically polarized light, at which point the extinction was  $\sim 100$  times worse than the polarizers themselves (Glan laser polarizers were measured to be  $5 \times 10^{-6}$ ). The worst extinction was  $2 \times 10^{-2}$  for horizontal polarization.

Eqs. 4.18 and 4.19 indicate that the signal to noise can be shot noise limited at  $\theta = \pi/2$ . However the small amount of light which makes it though both

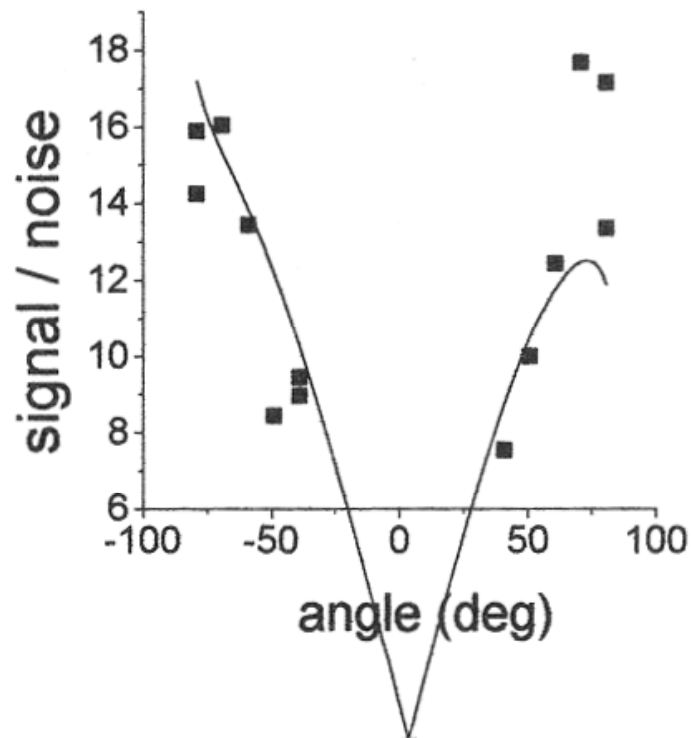


Figure 4.9: Plot of experimental signal to noise as a function of crossing angle  $\theta$  between the two polarizers. For this data  $\delta\phi = 3.6$  degrees. The solid line is a fit of the shot-noise limiting form.

polarizers (due to window birefringence and finite polarizer extinction) means that the minimum noise is the shot noise (or fractional noise) on this light. These comments are somewhat unnecessary though, since we must allow some light through in order to do a pixel by pixel calibration of the light intensity; the signal at each pixel is determined not only by the phase shift from the condensate, but also by spatial variations in probe intensity. These variations cannot be measured if  $\theta = \pi/2$ , without removing the second polarizer (which would no doubt result in a change in the spatial variations for a real-world polarizer). This is a general problem with dark-ground imaging schemes, even though they yield superior signal to noise in other applications (like polarization spectroscopy). It should be mentioned that schlieren [11] imaging does not suffer from this since high spatial frequency components do make it to the imaging plane.

### 4.3 Phase-contrast imaging

Phase-contrast imaging [12, 37] is another nondestructive technique currently in use. It relies on a comparison between the phase shifts of the light traveling through the condensate versus that which does not travel through. The effect may be derived using a straight forward argument (see Appendix A for a complete derivation).

At the plane perpendicular to the imaging axis, and just after the condensate, the electric field can be written as

$$E(x, t) = E_0 \cos(\omega t + \phi(x)) \quad (4.20)$$

where  $\phi(x)$  is a spatially dependent phase shift on the probe light from its interaction with the condensate. Assuming the phase shift is small this is

$$E(x, t) = E_0(\cos(\omega t) + \phi(x) \sin(\omega t)). \quad (4.21)$$

For small phase shifts this of course does not yield a signal since the time average of  $|E|^2$  does not depend on  $\phi(x)$ . We require an additional phase shift in only one of the terms in Eq. 4.21. If a  $\pi/2$  shift is applied to only the second term, then the intensity is

$$I(x) = I_0(1 + 2\phi(x)) \quad (4.22)$$

which reproduces the same phase pattern as that produced by the condensate.

Since the intensity is linearly dependent on the phase shift, the signal reverses signs depending on which side of resonance the probe beam is located. For a mixture of condensates in the  $|1, -1\rangle$  and  $|2, 1\rangle$  states, a beam tuned in the middle of the transitions gives a positive signal for  $|1, -1\rangle$  atoms and a negative signal for  $|2, 1\rangle$  atoms. When the states are spatially overlapping, the signal is proportional to the population difference.

The implementation is shown in figure 4.10. Light which is not affected by the condensate (solid lines) is focused at P1 by the first imaging lens. The part of the light which is diffracted by the condensate (dashed lines) is collimated at P1 since the condensate is at the focal point of the first lens. These two components are the two terms in Eq. 4.21. Since they are spatially separated by the lens, a  $\pi/2$  phase shift can be applied by inserting a window with a “phase dot” – a layer of MgF with the proper thickness. The diameter of the dot must be large compared to the waist size of the probe beam, but small compared to the diffracted beam. For our experiment with beam size  $\sim 2$  mm and condensate size  $\sim 20\mu\text{m}$ , the focused probe is  $50 \mu\text{m}$  and the diffracted beam is  $5000 \mu\text{m}$ , providing a large possible range for the phase dot size. We chose  $100 \mu\text{m}$  diameter in order to be able to image non-condensed atom clouds (at least the colder ones) that are much larger in size than the condensate.

In general it is not trivial to align the phase dot with the probe beam. The

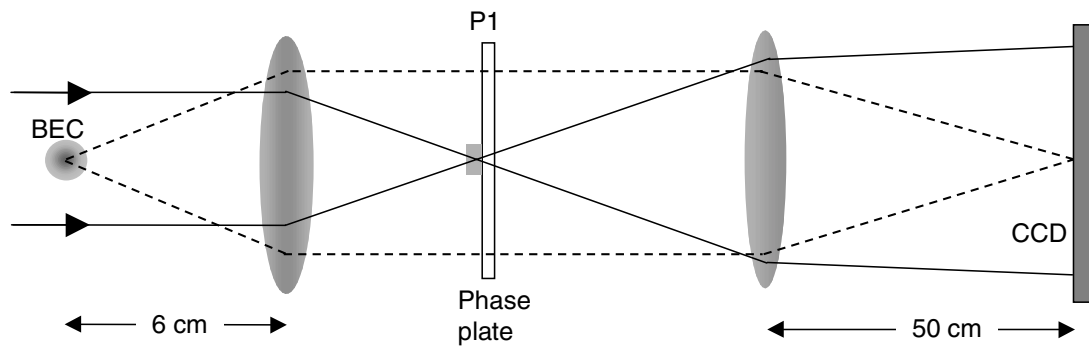


Figure 4.10: Schematic for phase contrast imaging. A probe beam is incident from the left, and obtains a spatially dependent phase shift from the condensate. It travels through the first imaging lens which focuses the probe light onto the phase dot at P1. The phase dot imparts a  $\pi/2$  phase shift to only the probe beam, but not to the diffracted light from the condensate. The second lens completes the microscope and images the condensate onto the CCD array.

most successful technique is to first place the dot so that it is not at the focal point of the first lens, so the dot does not encompass the focusing probe. A bull's eye pattern is then observed between the second lens and the CCD. As the phase dot is moved toward the beam focus the bull's eye pattern grows until, at the focus, the profile is flat.

### 4.3.1 Non-destructive imaging techniques

Both destructive and polarization imaging depend on atom orientation to define a symmetry axis. This is defined by the direction of the rotating TOP field. In the extreme case where the axis switches direction ( $1/2$  of a TOP period later), near-resonance imaging sees a large change in the detuning from resonance, and polarization imaging sees reversed Clebsch-Gordon coefficients, resulting in an opposite polarization rotation. Linearly polarized and far detuned, phase-contrast imaging gives nearly equal signals no matter which direction the TOP field points (see Table 4.1). Where the other methods require strobing of the probe light in order to wait for proper field alignment in the rotating TOP trap, phase-contrast images may be taken at any time, or even continuously.

Discrete, non-destructive pictures of a condensate are taken using kinetics mode of the Princeton Instruments camera (with ST138 controller). In this mode, the camera waits for either an internal or external trigger, at which time it advances the charge on each row of pixels by a set number of rows. A region of  $N$  rows may be defined as the exposed area by physically masking the remaining  $512 - N$  rows directly in front of the CCD. Once a trigger is received, the charge accumulated on the  $N$  rows is advanced into the unexposed area. This advancement occurs at a user-specified speed of  $19.2 \times (\text{integer multiples up to } 16) \mu\text{s}$  per row. Once the shift is complete the camera waits for a new trigger and repeats the process until the array is filled. The internal trigger mode has a fixed repetition

rate, but it is simple to provide arbitrary triggers in the external trigger mode. This latter method can be used to obtain any desired probe timing. Once the CCD is filled, the charge is read from the entire array, digitized and sent to the computer for analysis. In general, we are able to get  $\sim 12$  to 30 pictures of an individual condensate, depending on the condensate size (*i.e.* trap frequencies) and center-of-mass slosh. Figure 4.11 shows a non-destructive series of pictures of a condensate undergoing Rabi oscillations between the  $|2, 1\rangle$  and  $|1, -1\rangle$  states, with a Rabi period of about 5 images.

A semi-continuous movie may also be taken by scrolling the charge on the CCD at a constant rate (or, one can think of scrolling each row discretely as an individual frame). The scroll speed is still given by integer multiples of  $19.2 \mu\text{s}$  per row for internal triggering, which means that the total time ranges from 10 ms to 157 ms. External triggers again enable arbitrarily long frames. Since the condensate image occupies many pixel rows, this method smears out vertical (along the direction of scrolling) density information. However, it is extremely useful for quickly measuring center-of-mass slosh, and quantitatively useful in measuring Rabi frequencies. Figure 4.12 shows a continuous movie of (a) a condensate undergoing Rabi oscillations between the  $|2, 1\rangle$  and  $|1, -1\rangle$  states, and (b) radial and axial center-of-mass slosh.

### 4.3.2 Signal to noise

Assuming the phase dot thickness is  $\pi/2$  and  $\phi$  is small, the signal to noise in phase-contrast is

$$S/N_{\text{shot}} = \frac{\sqrt{I_0}\phi}{\sqrt{(\phi+1)(\phi+2)}} \quad (4.23)$$

for shot noise, and for “fringe noise” it is

$$S/N_{\text{fringe}} = \frac{\phi\sqrt{2}}{A(\phi+1)\sigma} \quad (4.24)$$

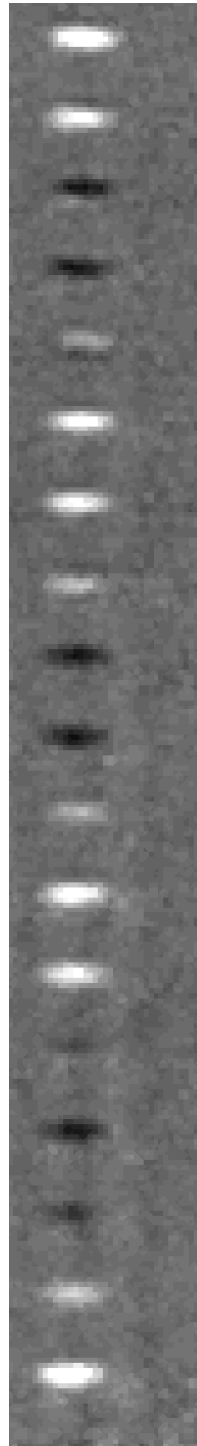


Figure 4.11: Discrete, non-destructive imaging of a condensate undergoing Rabi oscillations. For each image, the probe beam is flashed on and off quickly, and the resulting CCD charge scrolled away from the exposed area. The phase contrast signal is positive (white) for the  $|1, -1\rangle$  state and negative (black) for the  $|2, 1\rangle$  state. The two-photon drive is on during for the duration of the images.

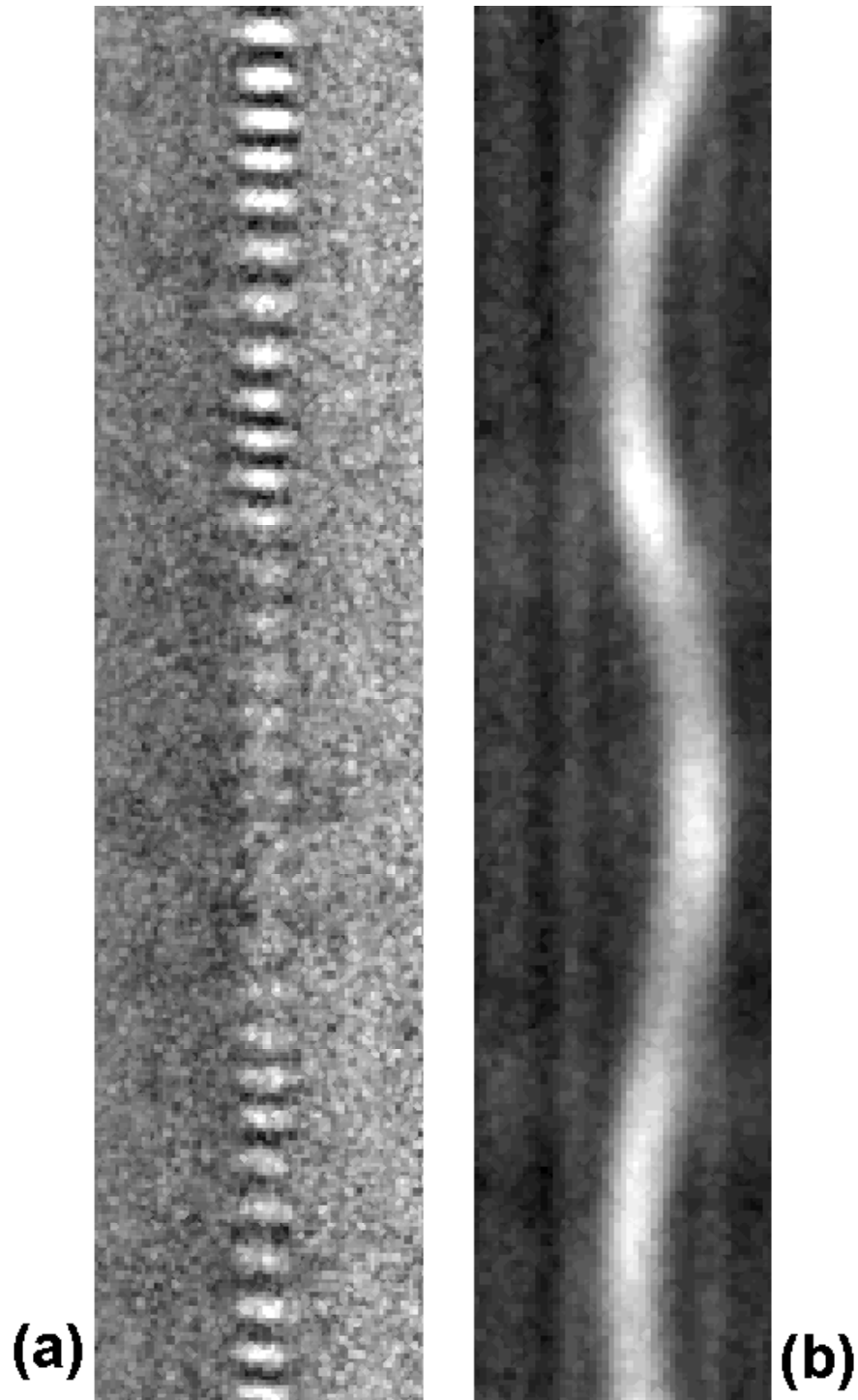


Figure 4.12: Continuous, non-destructive images. (a) A condensate undergoing Rabi oscillations (with collapse and revival). (b) A single condensate in the  $|1, -1\rangle$  state oscillating radially (horizontally in the picture) and axially (vertically in the picture). The axial oscillation is manifested as an increase (decrease) in the signal as the condensate moves with (against) the CCD scrolling.

The shot noise limit was experimentally observed in figure 4.13 for a trapped condensate in a 62 Hz axial trap.

#### 4.4 Comparisons

The next section compares the three imaging techniques based on their usefulness for a specific measurement. The criteria are measurement of density distributions, signal to noise, double condensate signal, and non-destructive movies.

Single and two-state condensate density distributions are best imaged after ballistic expansion with destructive imaging. The main reason is that the imaging resolution is  $\sim 5\mu\text{m}$ , too small for a common  $10\mu\text{m}$  cloud (although reasonable for  $50\mu\text{m}$  condensates in very weak traps). With destructive imaging we are sensitive to  $< 5\%$  deviations in overall condensate size when looking at collective excitations. The major drawback here is that time dependence cannot be studied using a single condensate; each time step point must be taken with a fresh condensate, requiring more experiment stability. It is also necessary to mathematically reconstruct the condensate's image as it was in the trap before expansion using the nonlinear Schrödinger equation. However, qualitative reconstruction is generally possible using scaling and scattering length arguments.

Signal to noise in overall condensate number is generally the best for polarization imaging in the trap. This is the case when the noise is dominated by spatial intensity fluctuations on the probe laser since the polarizers may be crossed to eliminate background light. In order to get spatial information, the profile of the probe must be flat on the scale of the condensate in order to forgo the background subtraction which is not possible for crossed polarizers. If the imaging resolution is larger than the condensate, then it is better to destructively image a dropped cloud near resonance.

Phase-contrast is the best technique for double condensate imaging and for

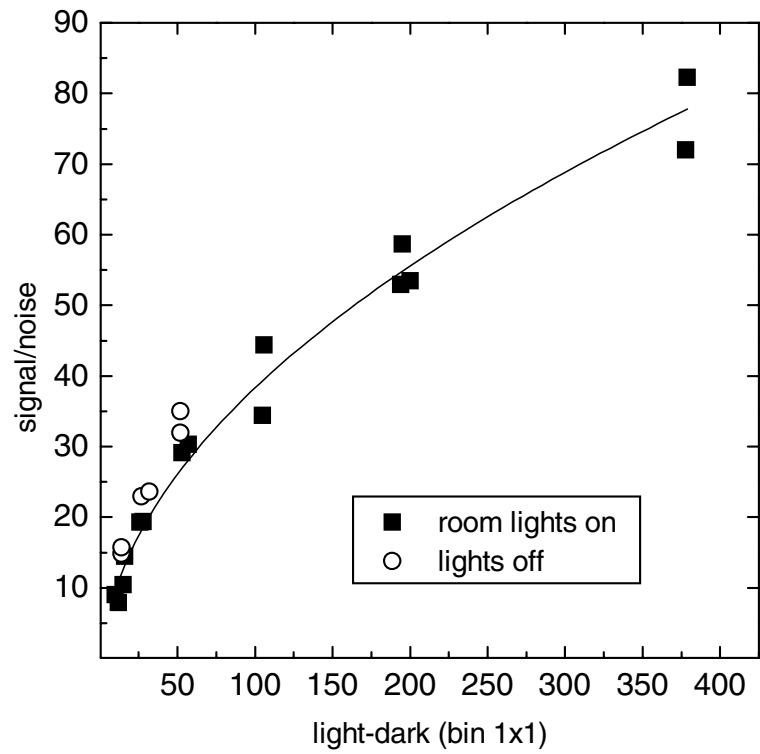


Figure 4.13: Plot of the experimental signal to noise of a condensate in the trap, as a function of probe light level  $I$  for phase contrast imaging. The solid line is a fit to the shot noise limit which is proportional to  $\sqrt{I}$ .

multiple images of the same condensate. Although polarization imaging has better signal to noise for crossed polarizers, no state specific information is possible (both + and - polarization rotations give the same signal) in that configuration. Phase-contrast is still better than polarization (with uncrossed polarizers) due to its smaller dependence on magnetic field direction.

The biggest noise contribution is usually spatial variations in the beam intensity that change position between the condensate picture and the background picture. These seem to be due to interference implanted by multiple reflections from optical surfaces, or diffraction from aperaturing of the beam or from small imperfections on the optics (dust for example). The size scale is often near the scale of whatever is being imaged, which seems to indicate that multiple patterns and sizes are present. There are a few techniques which have helped to diminish the effect of the stripes. Changing the alignment of optics (beamsplitters, polarizers) before and after the trap has helped. Occasionally, changing the magnetic trap parameters from the condensate image to the background image has an effect. Since the rotating magnetic field produces audible noise, it causes vibrations in the optics and windows, which modulates the fringe pattern. It has helped to find specific phases and amplitudes of the rotating field to minimize the difference between the two frames.